Composite Structures 337 (2024) 118084

Contents lists available at ScienceDirect

Composite Structures

journal homepage: www.elsevier.com/locate/compstruct

In-situ failure behavior and interfacial bonding of an interpenetrating metal matrix composite reinforced with lattice-like metallic glass ($Ni_{60}Nb_{20}Ta_{20}$) preform

Kerstin Dittmann [a,*], Robert Gruhl [b], Anna Trauth [a], Kay André Weidenmann [a]

[a] Institute of Materials Resource Management (MRM), Augsburg University, Am Technologiezentrum 8, 86159 Augsburg, Germany
[b] Experimental Physics VI, Center for Electronic Correlations and Magnetism, Augsburg University, Universitätsstraße 1, 86159 Augsburg, Germany

ARTICLE INFO

Keywords:
Interpenetrating Metal Matrix Composite (IMMC)
Metallic glass (MG)
In-situ compression testing
$Ni_{60}Nb_{20}Ta_{20}$
Scanning electron microscopy

ABSTRACT

Metallic glasses (MG) have an amorphous atomic structure and exhibit several exceptional properties such as high strength, hardness associated with high elastic strain limit and elastic energy storage. But MGs are also prone to brittle fracture, making them difficult to use as monolithic structural components and might better be used as a reinforcement phase in hybrid composites such as metal matrix composites (MMC). The failure behavior of composites depends on the structure of the reinforcement phase. In this work, the failure behavior of an interpenetrating MMC reinforced with a MG ($Ni_{60}Nb_{20}Ta_{20}$) lattice-like preform and AlSi12-matrix was investigated by in-situ compression tests under scanning electron microscopy to get a better understanding of the influence of the lattice-like preform and mechanical interference between both phases. Additionally, microstructure analysis by scanning transmission electron microscopy and energy dispersive X-ray measurements were carried out to gain insight into the chemical composition of the interfaces. The failure behavior in manufacturing direction of the MMC is dominated by shear stress whereas transversely to manufacturing direction by normal stress and exhibits therefore an anisotropic failure behavior. Investigations of the interfaces show more of a mechanical than chemical bonding but in general a good interfacial bonding was confirmed.

1. Introduction

Metallic glasses, also known as amorphous metals or glassy metals, are a unique class of materials that, unlike conventional metals with a crystalline structure, have a non-crystalline (amorphous) atomic structure. Due to this structure, they exhibit several exceptional properties, such as high strength, hardness, and corrosion resistance associated with high elastic strain limits and the possibility of high elastic energy storage [1–3]. However, the amorphous structure also causes low ductility and metallic glasses are therefore susceptible to brittle fracture. This makes them difficult to use as monolithic structural components [4], which is why they are often used as a reinforcement phase in a hybrid material, such as a metal matrix composite (MMC). The ductile matrix partially compensates for the brittleness of the reinforcement phase, resulting in more predictable failure behavior [5–7].

MMCs are hybrid materials characterized by a macroscopic composite structure combining a metallic matrix with a reinforcement phase. In MMCs, the usual reinforcement phases are ceramic materials embedded mainly in a lightweight metal matrix [8]. The reinforcement phase can be in different forms, such as particles, fibers, or three-dimensional structures. Three-dimensional structures are often referred to as interpenetrating composites, meaning that each component in the composite is topologically interconnected throughout the entire material volume [9]. MMCs have the potential to outperform the mechanical properties of monolithic components. These improvements are particularly evident in terms of specific stiffness, creep resistance, and fatigue behavior [8,10,11]. By using metallic glass as a reinforcement phase, the strength and Young's modulus of the metallic matrix is also increased, which has been proven in several studies [5,12,13], while maintaining the ability of plastic deformation under compressive load [14]. The failure behavior under mechanical compression depends on the structure of the reinforcement phase. In [13,15], metallic glass platelets of Ni-Nb-Ta alloy were used to reinforce a AlSi12-matrix. The failure behavior of the MMC under compression was studied in in-situ

* Corresponding author at: Chair of Hybrid Composite Materials, Institute of Materials Resource Management (MRM), Augsburg University, Am Technologiezentrum 8, 86159 Augsburg, Germany.
E-mail address: kerstin.dittmann@mrm.uni-augsburg.de (K. Dittmann).

https://doi.org/10.1016/j.compstruct.2024.118084
Received 6 October 2023; Received in revised form 14 February 2024; Accepted 27 March 2024
Available online 28 March 2024

compression tests and a dependence on the orientation of the metallic glass platelets was observed.

In addition, essential for good mechanical properties is the interfacial bonding between the two phases in a hybrid material, because at the interfaces the load transfer from the matrix to the reinforcement phase occurs. MMCs with metallic glasses as reinforcement phase in general exhibit good interfacial bonding due to the metallic character of both phases [8,16–18]. In several studies [16,19,20] the interfacial bonding in MMCs with metallic glasses have already been investigated and it was shown that temperature during the manufacturing process of the composite has a great influence on the interfacial bonding. If the MMC is manufactured without temperature influence, for example by electrolytic deposition of the matrix material [16] or by cold forming [19], no interfacial bonding develops. Whereas MMCs manufactured at higher temperatures or had a heat treatment exhibit good interfacial bonding [16]. According to [16], the good interfacial bonding occurs due to the formation of an interdiffusion layer at the interfaces. Additional to an interdiffusion layer, good interfacial bonding can also be achieved by mechanical bonding [8]. Mechanical bonding occurs through a rough surface of the reinforcement phase, enabling mechanical keying with the matrix material.

In this work, the elastic–plastic deformation and damage behavior of an interpenetrating MMC was investigated by mechanical in-situ compression tests in a scanning electron microscope (SEM). The MMC is reinforced with a metallic glass lattice-like structure with alloy composition $Ni_{60}Nb_{20}Ta_{20}$ and manufactured by a laser powder bed fusion (LPBF) process according to [21]. This manufacturing process both enables to control the (an-)isotropy of the interpenetrating MMC and features a certain micro-roughness enhancing the interfacial bonding representing a novel approach. The composite was manufactured by infiltrating the metallic glass lattice structure with a eutectic AlSi12-matrix in a gas pressure infiltration process according to [22]. During the in-situ investigations, special attention was paid to the influence of the lattice-like geometry of the metallic glass on the damage behavior of the MMC as well as the interfacial bonding between the metallic glass and matrix material. To get a better understanding of the interfacial bonding and its chemical composition, scanning transmission electron microscopy (STEM) images were taken and energy dispersive X-ray spectroscopy (EDX) measurements were carried out. To the authors best knowledge, this is the first time that the failure behavior of an MMC with this material system ($Ni_{60}Nb_{20}Ta_{20}$-AlSi12) has been investigated by in-situ compression tests and EDX measurements in a TEM. In addition, the correlation between the mechanical failure behavior and the structure of the interface between the metallic glass and the aluminum alloy was investigated and discussed in detail.

2. Experimental

2.1. Materials and composite manufacturing

In the study at hand, an interpenetrating metal matric composite (MMC) reinforced with metallic glass and an aluminum matrix was investigated. The metallic glass alloy has a nominal composition of $Ni_{60}Nb_{20}Ta_{20}$ (TaNi39.1Nb20.7 wt-%) and was produced by an induction melting process of the elements with a purity of 99.5 % by Fraunhofer Institute IFAM (Dresden, Germany). To obtain its amorphous structure, it was further processed by Nanoval GmbH & Co.KG (Berlin, Germany) by powder gas atomization, resulting in an amorphous powder with particle size d50 = 44 µm. The amorphous powder was further processed into an open-porous lattice-like structure with an open porosity of 63 % by laser powder bed fusion (LPBF) conducted in cooperation with the research group "Production and Component Behavior" at the Institute for Applied Materials – Materials Science and Engineering, Karlsruhe Institute of Technology (KIT, Karlsruhe, Germany). A detailed description of the manufacturing process of the lattice-like preform is given in [21]. To manufacture the interpenetrating MMC, the open-porous preform was infiltrated with an AlSi12 eutectic aluminum alloy in a gas pressure infiltration process. Since the metallic glass alloy $Ni_{60}Nb_{20}Ta_{20}$ exhibits a high crystallization temperature of 694 °C [21] and the AlSi12 a low melting temperature of 577 °C [23], a corresponding process temperature of 660 °C was chosen to keep the amorphous structure of the metallic glass. For a detailed description of the infiltration process and the resulting properties of the MMC, the authors refer to [22].

2.2. Sample preparation and in-situ testing setup

The investigated samples have a cubic geometry with a final edge length of approximately 3.5 mm. For this purpose, cubes with an initial edge length of 5 mm were cut from the composite using a diamond wiresaw by Diamond WireTec GmbH & Co.KG (Weinheim, Germany) and then manually grinded with abrasive SiC grinding paper of P1200 with a Tegramin 25 grinding machine by Struers GmbH (Willich, Germany) until the desired geometry with plane parallel surfaces was achieved. The surface to be examined was finally polished following the method published in [22] which is displayed in Table 1. Sputtering the sample was not necessary.

For the in-situ investigations an in-situ compression device from Kammrath & Weiss GmbH (Schwerte, Germany) with a 10 kN load cell was used. The displacement is recorded using a linear glass scale attached to the module and has a resolution of 0.1 µm. The compression device with an installed sample and a prepared sample are shown in Fig. 1.

For the experiments, the compression device was installed in the vacuum chamber of a scanning electron microscope Prisma E SEM from ThermoFisher Scientific (Waltham, Massachusetts, USA). The compression tests were performed with crosshead velocity of 0.5 µm/s, corresponding to a nominal strain rate of $d\varepsilon/dt = 1.43 \bullet 10^{-4}$ 1/s according to the sample geometry used. To take high-resolution SEM images of the deformation and damage behavior, the experiment was stopped and the changes in the microstructure were documented.

2.3. Transmission electron microscopy setup and sample preparation

For microstructure analysis scanning transmission electron microscopy (STEM) and energy dispersive X-ray spectroscopy (EDX) measurements were carried out using a JEOL JEM-ARM200F NEOARM transmission electron microscope (TEM) from JEOL GmbH (Freising, Germany) operated at 200 kV. Bright field (BF) and high-angle annular dark field (HAADF) detectors were used to acquire STEM images of the interface between the metallic glass $Ni_{60}N_{20}Ta_{20}$ and the AlSi12 alloy. EDX measurements were performed to gain insight into the chemical composition.

The TEM lamella was prepared by focused ion-beam lift-out technique using a ZEISS Crossbeam 550 from ZEISS (Oberkochen, Germany) equipped with a 30 kV Ga beam and an additional scanning electron

Table 1
Polishing steps to prepare the surfaces for in-situ investigations according to [22].

Grinding paper/ polishing cloth	Suspension	Contact pressure(N)	Circulation (rpm)	Time (min)
SiC (P1200)	Water	25	Co-rotation 150/150	5:00
MD-Largo	Diamond, 9 µm	25	Co-rotation 150/150	3:30
MD-DAC	Diamond, 3 µm	20	Co-rotation 150/150	3:30
MD-DUR	Diamond, 1 µm	10	Co-rotation 100/110	3:30
MD-CHEM	OP-S	10	Counter-rotation 150/150	1:10

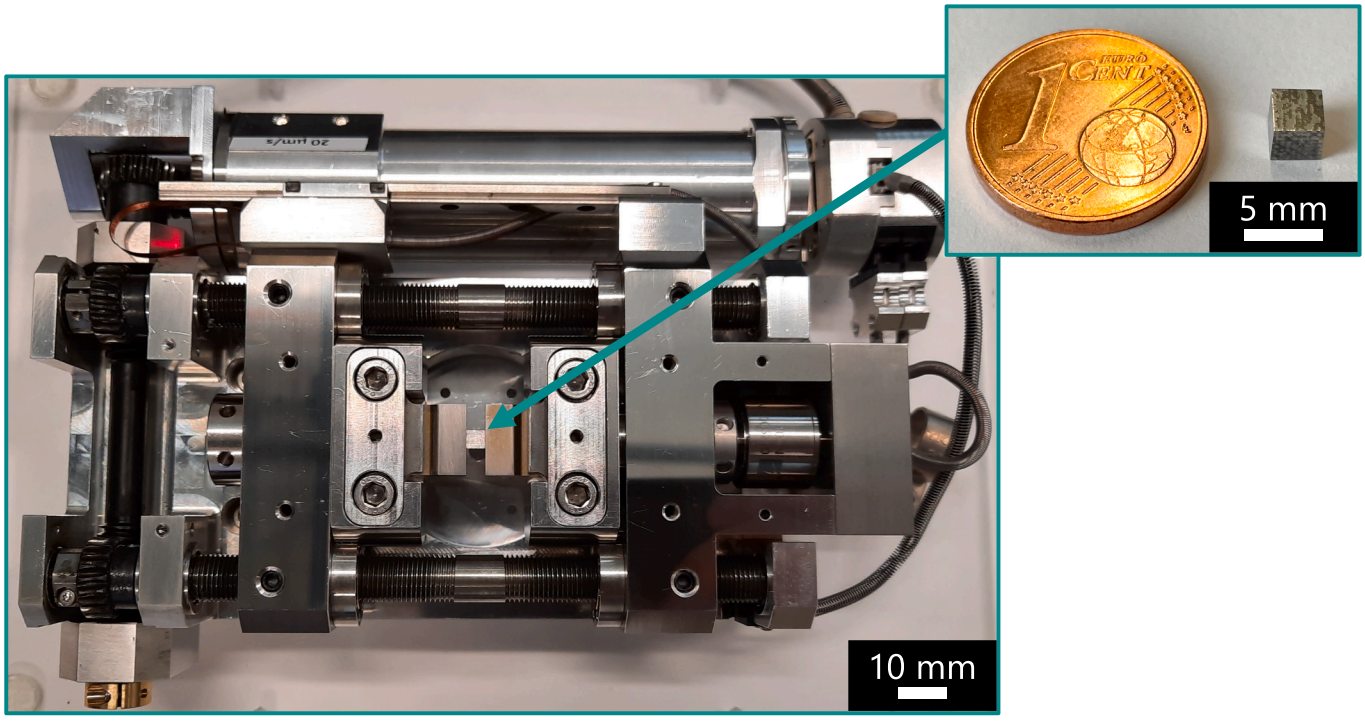

Fig. 1. In-situ compression device by Kammrath & Weiss with installed sample (figure by [24]) and close-up of a prepared MMC sample compared to a cent coin.

microscope (SEM). The region of interest was chosen at the interface of the metallic glass and the aluminum alloy. To protect the surface of the sample a 3 µm Pt-layer was deposited with a gas injection system. Lift-out and thinning of the lamella was carried out at 30 kV followed by two cleaning steps at lower energies of 5 kV and 2 kV respectively.

3. Experimental results

3.1. In-situ compression investigations

Preliminary investigations performed on the $Ni_{60}Nb_{20}Ta_{20}$-AlSi12 MMC, that were published by the authors in [22], show that the composite exhibits an inhomogeneous structure in and transversely to the

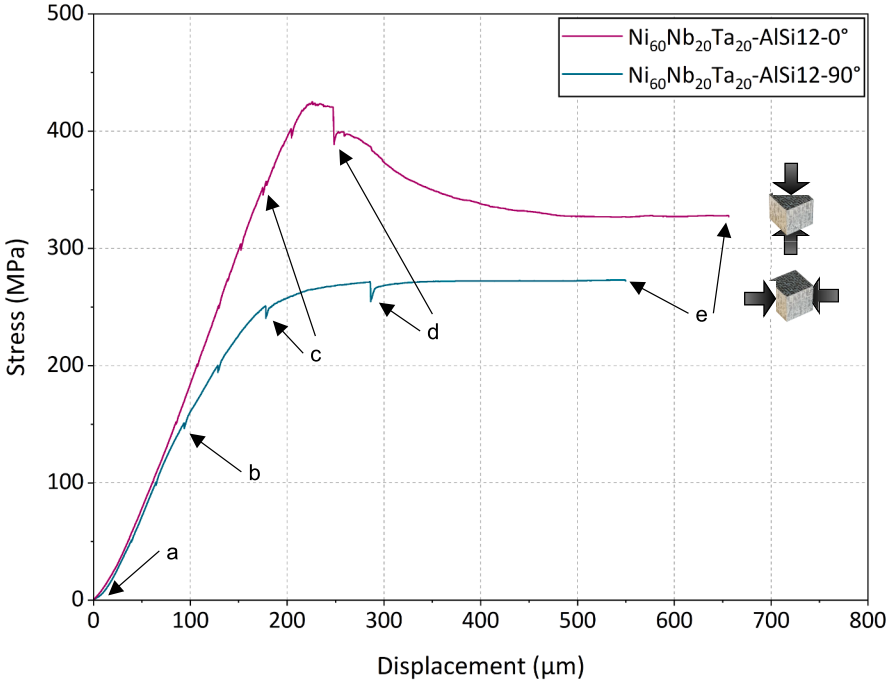

Fig. 2. Resulted stress-displacement diagram of one sample tested in infiltration direction named $Ni_{60}Nb_{20}Ta_{20}$-AlSi12-0° and one sample tested transversely to infiltration direction named $Ni_{60}Nb_{20}Ta_{20}$-AlSi12-90° by in-situ compression tests. The arrows indicate the holding points at which the high-resolution SEM images were taken.

manufacturing direction, which is due to the laser-based manufacturing process of the $Ni_{60}Nb_{20}Ta_{20}$ lattice-like preform.

Therefore, the in-situ compression tests were performed in manufacturing direction named $Ni_{60}Nb_{20}Ta_{20}$-AlSi12-0° and transversely to manufacturing direction named $Ni_{60}Nb_{20}Ta_{20}$-AlSi12-90°. Several samples were tested in both directions, but as they all show the same failure behavior, the results of only one representative sample are presented in the following. The resulting stress-displacement curves are shown in Fig. 2. The displacement is given in micrometer, measured by the linear glass scale of the compression module. To take high-resolution SEM images of the microstructure, the compression test had to be interrupted which is reflected in the recorded curve by a drop in stress due to relaxation. The holding points are indicated by arrows. The MMC in 0°-direction reaches a maximum compressive strength of 420 MPa, whereas the MMC in 90°-direction is significantly lower at 270 MPa. Additionally, the two samples show a remarkably different failure behavior under maximum compression. At first a similar linear increase is observed for both samples. After reaching 150 MPa, the curve of the $Ni_{60}Nb_{20}Ta_{20}$-AlSi12-90° sample begins to flatten out before reaching the maximum compressive strength. Upon reaching the maximum, the curve ends in a constant plateau until the experiment is manually stopped. Whereas the curve of the $Ni_{60}Nb_{20}Ta_{20}$-AlSi12-0° sample continues to increase to the maximum compressive strength and decreases directly afterwards until it reaches a constant plateau at 330 MPa.

In the following, the visual results of the in-situ compression test on the $Ni_{60}Nb_{20}Ta_{20}$-AlSi12-0° MMC sample carried out along the manufacturing direction are presented. Fig. 3 shows the overview SEM images taken at (a) the beginning. (d) the maximum compressive strength and (e) the end of the experiment. The figure labelling has been chosen to correlate with the stress-displacement diagram in Fig. 2. In (a) the area is marked where the close-up images of the microstructure were taken during the experiment.

The close-up images of the microstructure were taken at selected load levels of 150 MPa, 350 MPa, 420 MPa and at the end of experiment and are shown in Fig. 4. The first holding point was at (b) 150 MPa and thus in the middle of the linear-elastic range. No visible damage occurred yet, except of already existing cracks in the $Ni_{60}Nb_{20}Ta_{20}$ phase due to the manufacturing and preparation process of the sample, marked by yellow arrows. Those cracks propagate in the metallic glass under increasing stress, as can be seen in (b) at 350 MPa and the end of the linear-elastic range. In addition, new cracks develop in the metallic glass phase (yellow arrows), while plastic deformation is visible in the AlSi12-matrix (white arrows) and local debonding along the phase boundary between the $Ni_{60}Nb_{20}Ta_{20}$ metallic glass phase and AlSi12-matrix is initiated (pink arrows). The plastic deformation in the AlSi12-matrix occurs mainly due to debonding at the interfaces of the Si-lamellae and the primary silicon precipitates to the α-aluminum. Additionally, the Si-lamellae and primary silicon precipitates start to fracture. When reaching the maximum compressive strength at (d) 420 MPa total failure occurs in both phases due to brittle fracture in the metallic glass (yellow arrows), the Si-lamellae and the primary silicon precipitates as well as debonding between those phases and the α-aluminum (white arrows). At the end of the experiment in (e), it is observed that failure occurs in the AlSi12-matrix and along the interfaces with the metallic glass due to shear stress in 45°-direction with respect to the compression direction (white arrows). Whereas the metallic glass phase exhibits brittle failure due to normal stress along compression direction (yellow arrows). Additionally, it can be observed that debonding between the metallic glass and the AlSi12-matrix occurs comparatively less and the interfaces stay mostly intact at a microscopic level (pink arrows).

In Fig. 5 the results of the in-situ compression test on the $Ni_{60}Nb_{20}Ta_{20}$-AlSi12-90° MMC sample carried out transversely to manufacturing direction at (a) the beginning, (d) the maximum compressive strength and (e) the end of experiment are shown. Again, the area of close-up images of the microstructure is marked in (a) and the labelling of the figures has been chosen to correlate with the stress-displacement diagram in Fig. 2.

The close-up images of the microstructure were taken at selected load levels of 150 MPa, 250 MPa, 260 MPa and at the end of experiment and are displayed in Fig. 6.

The first holding point was in the linear-elastic range at (b) 150 MPa. No damage occurred expect of already existing cracks in the $Ni_{60}Nb_{20}Ta_{20}$ metallic glass phase due to the manufacturing and sample preparation process, marked by yellow arrows. Increasing the stress to (c) 250 MPa, already existing cracks start to propagate, and new cracks occur in the metallic glass (yellow arrows). For the AlSi12-matrix, the same behavior as in the $Ni_{60}Nb_{20}Ta_{20}$-AlSi12-0° sample can be observed. It exhibits plastic deformation causing debonding at the interfaces of the Si-lamellae and the primary silicon precipitates to the α-aluminum and cracks occur within the lamellae and precipitates (white arrows). Local debonding between the metallic glass phase and AlSi12-matrix cannot yet be observed. But at maximum stress at (d) 270 MPa some local areas exhibit debonding, marked by pink arrows. Additionally, total failure occurs in the metallic glass phase (yellow arrows) due to brittle fracture and in the AlSi12-matrix due to plastic deformation and brittle fracture in the Si-lamellae and the primary silicon precipitates. At the end of experiment (e), the same behavior in total failure can be observed as in the $Ni_{60}Nb_{20}Ta_{20}$-AlSi12-0° sample. The AlSi12-matrix fails due to shear stress in 45° direction as well as due to debonding at the interfaces between the metallic glass phase and matrix (white arrows). The metallic glass phase fails due to normal stress along compression direction (yellow arrows). Again, debonding between the metallic glass and AlSi12-matrix occurs comparatively less and most of the interfaces stay intact (pink arrows).

3.2. TEM investigations

In the following section, the results of the TEM investigations performed on the MMC at the interface between the metallic glass $Ni_{60}Nb_{20}Ta_{20}$ and the AlSi12-matrix are presented. Fig. 7 shows the interface recorded in (a) bright field (BF) and (b) high angle annular

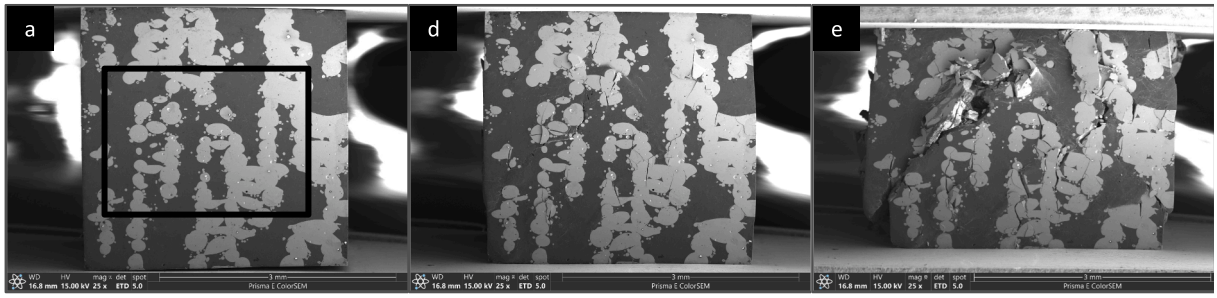

Fig. 3. Overview SEM images of the $Ni_{60}Nb_{20}Ta_{20}$-AlSi12-0° sample tested in manufacturing direction at (a) the beginning with the marked area where close-up images are taken, (d) the maximum compressive strength and (e) the end of experiment.

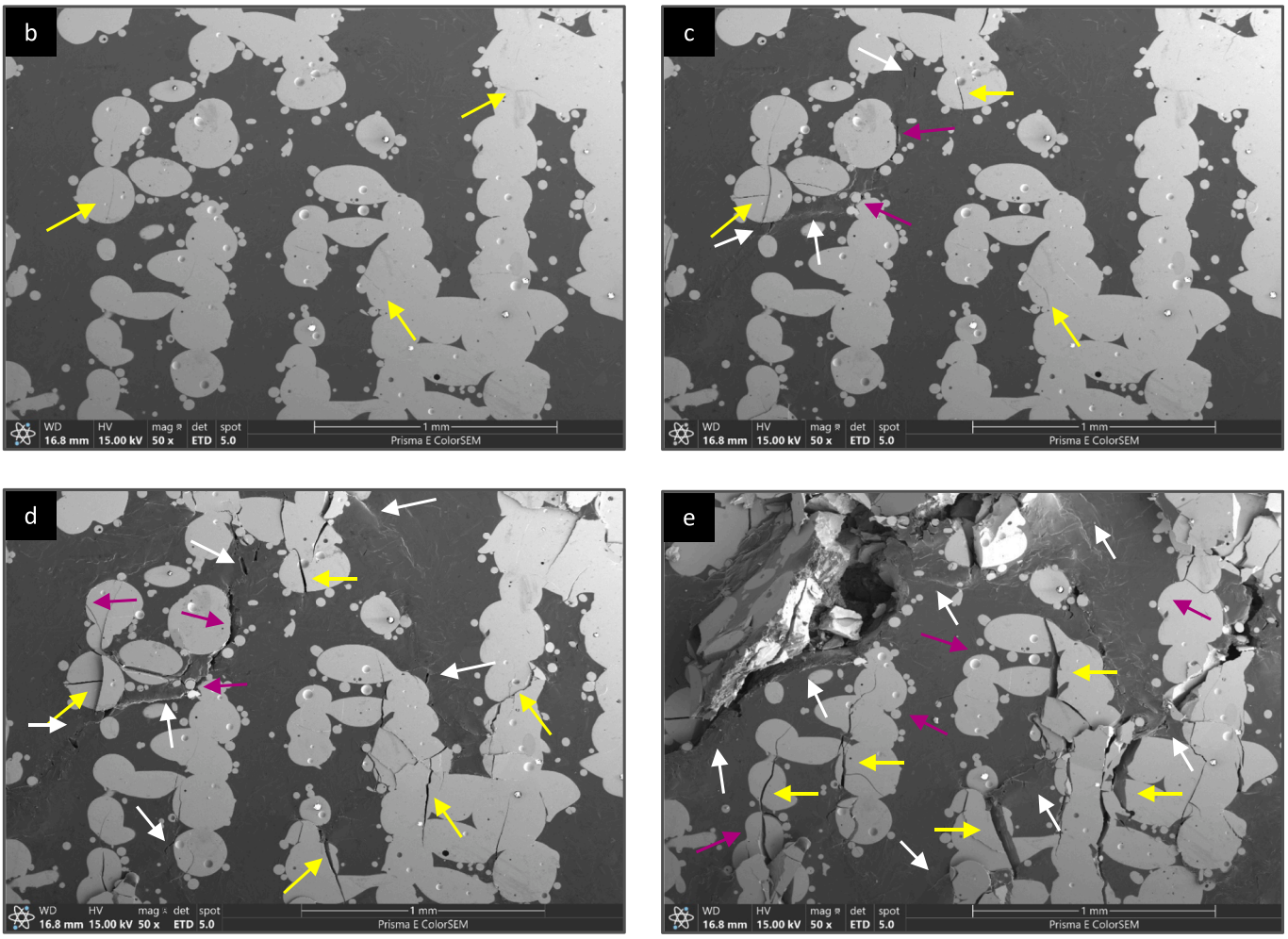

Fig. 4. Close-up SEM images of the $Ni_{60}Nb_{20}Ta_{20}$-AlSi12-0° sample tested in manufacturing direction at (b) 150 MPa, (c) 350 MPa, (d) 420 MPa and (e) the end of experiment.

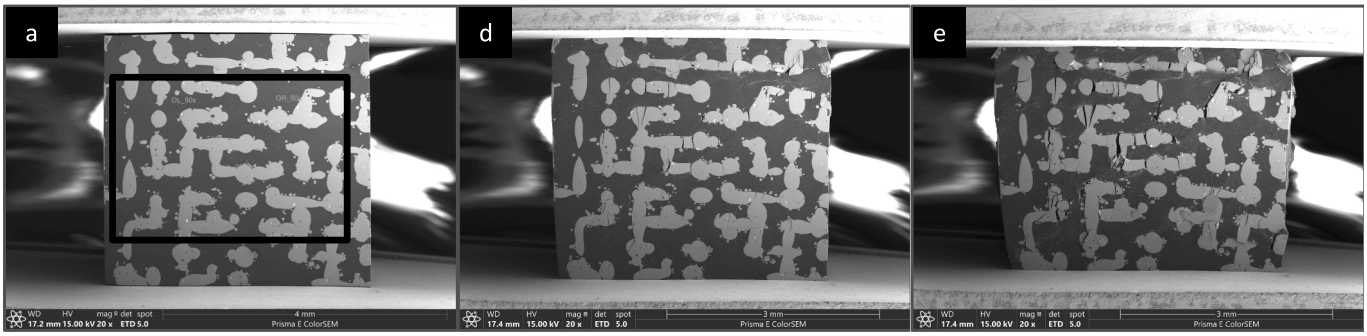

Fig. 5. Overview SEM images of the $Ni_{60}Nb_{20}Ta_{20}$-AlSi12-90° sample tested transversely to manufacturing direction at (a) the beginning with the marked area where close-up images are taken, (d) the maximum compressive strength and (e) the end of experiment.

dark field (HAADF-) modes. In HAADF mode the metallic glass appears bright, while in BF mode it is completely dark. In the STEM images, the location of the EDX line scan is marked. The result of the EDX line scan is presented in a diagram in (c). In general, the interface between the two phases appears rough which is due to the primary silicon precipitates located at the interface. Neither in HAADF nor in BF mode is a reaction layer visible between the two phases, which could have been formed during the infiltration process. The resulting EDX line scan confirms the visual evaluation The scan starts in the $Ni_{60}Nb_{20}Ta_{20}$ phase with a high intensity of nickel and lower intensity of niobium and tantalum. In addition, some silicon is detected which is probably a misidentification of the EDX scan and will be further discussed in the next section. Approaching the interface at 0.8 µm the element content of Ni, Nb and Ta decrease to zero while the Si content increases. Also, a slight increase in oxygen and aluminum can be observed in the interface area (between 0.75 µm and 1.0 µm) superimposed with the elements of the metallic glass, leading to the suggestion that some minor diffusion into the metallic glass phase has occurred. Both elements decrease at 1 µm again, whereas the silicon continues to increase. At 1.75 µm, the silicon decreases again and an increase in aluminum can be observed. This

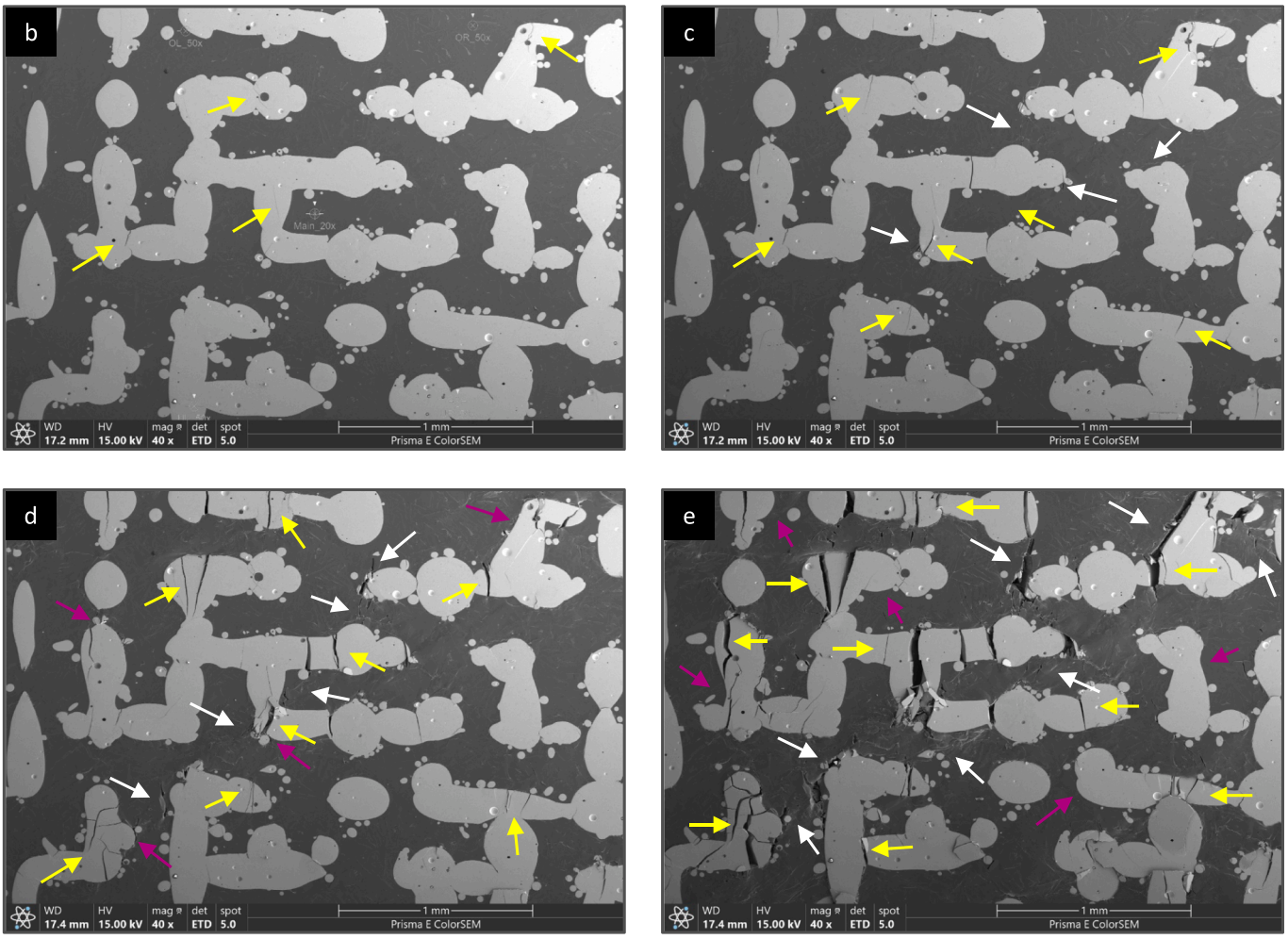

Fig. 6. Close-up SEM images of the $Ni_{60}Nb_{20}Ta_{20}$-AlSi12-90° sample tested transversely to manufacturing direction at (b) 150 MPa, (c) 250 MPa, (d) 270 MPa and (e) the end of experiment.

confirms that a primary silicon precipitate embedded in α-aluminum has accumulated to the interface.

4. Discussion

4.1. Failure behavior under compression

The sample $Ni_{60}Nb_{20}Ta_{20}$-AlSi12-0° tested in manufacturing direction exhibits with 420 MPa significantly higher maximum compressive strength then the sample $Ni_{60}Nb_{20}Ta_{20}$-AlSi12-90° tested transversely to manufacturing direction and only exhibits a compressive strength of 270 MPa. These results correlate with the results of mechanical compression tests performed ex-situ on the same material $Ni_{60}Nb_{20}Ta_{20}$-AlSi12 MMC as published by the authors in [22], where the samples in 0°-direction reaches a maximum compressive strength of 430 MPa and in 90°-direction of 280 MPa. The significant difference is due to the anisotropic $Ni_{60}Nb_{20}Ta_{20}$-lattice structure caused by the laser-based manufacturing process [21,22]. Both samples show already existing cracks in the linear-elastic range in the $Ni_{60}Nb_{20}Ta_{20}$ phase. This is probably due to the sample preparation process and can be confirmed by comparing the SEM images with micrographs of the microstructure of the same $Ni_{60}Nb_{20}Ta_{20}$-AlSi12 MMC in [22], where no cracks are visible in the microstructure of the $Ni_{60}Nb_{20}Ta_{20}$ phase.

In the study at hand, both samples feature a brittle failure behavior of the reinforcement phase and ductile failure behavior of the matrix phase. Similar behavior has been observed in other MMCs reinforced with metallic glass [14,25]. In [13,15], the same material system ($Ni_{60}Nb_{20}Ta_{20}$-AlSi12) was studied, but instead of an interpenetrating lattice structure, the metallic glass featured a platelet structure representing a particle reinforced MMC. There, a dependence of the maximum compressive strength and the failure behavior on the orientation of the metallic glass platelets was also observed. In [13] ex-situ compression tests were carried out and samples tested along the orientation of the platelets exhibit higher compressive strength compared to the samples tested transversely to the platelets direction. In [15], samples with a similar reinforcement fraction of 36 % were investigated regarding the failure behavior by in-situ compression tests and exhibit a similar failure behavior as the samples tested in the study at hand. It occurs debonding at the interfaces between the primary silicon precipitates and Si-lamellae to the α-aluminum and brittle fractures in the metallic glass and the silicon. Like the samples tested in the study at hand, the metallic glass phase fails due to normal stress parallel to load direction no matter the sample is tested along or transversely to the platelet's orientation. Samples tested along the orientation of the platelets can be compared to the samples tested along the manufacturing direction ($Ni_{60}Nb_{20}Ta_{20}$-AlSi12-0°) in this work. In both cases the AlSi12-matrix fails due to shear stress in 45°-direction to the load direction and shearing of the entire sample can be observed. But whereas in [15] debonding between the metallic glass and the α-aluminum occurs parallel to the load direction, in the study at hand debonding occurs along the 45°-direction. The samples tested transversely to the orientation of the platelets can be compared with the samples tested

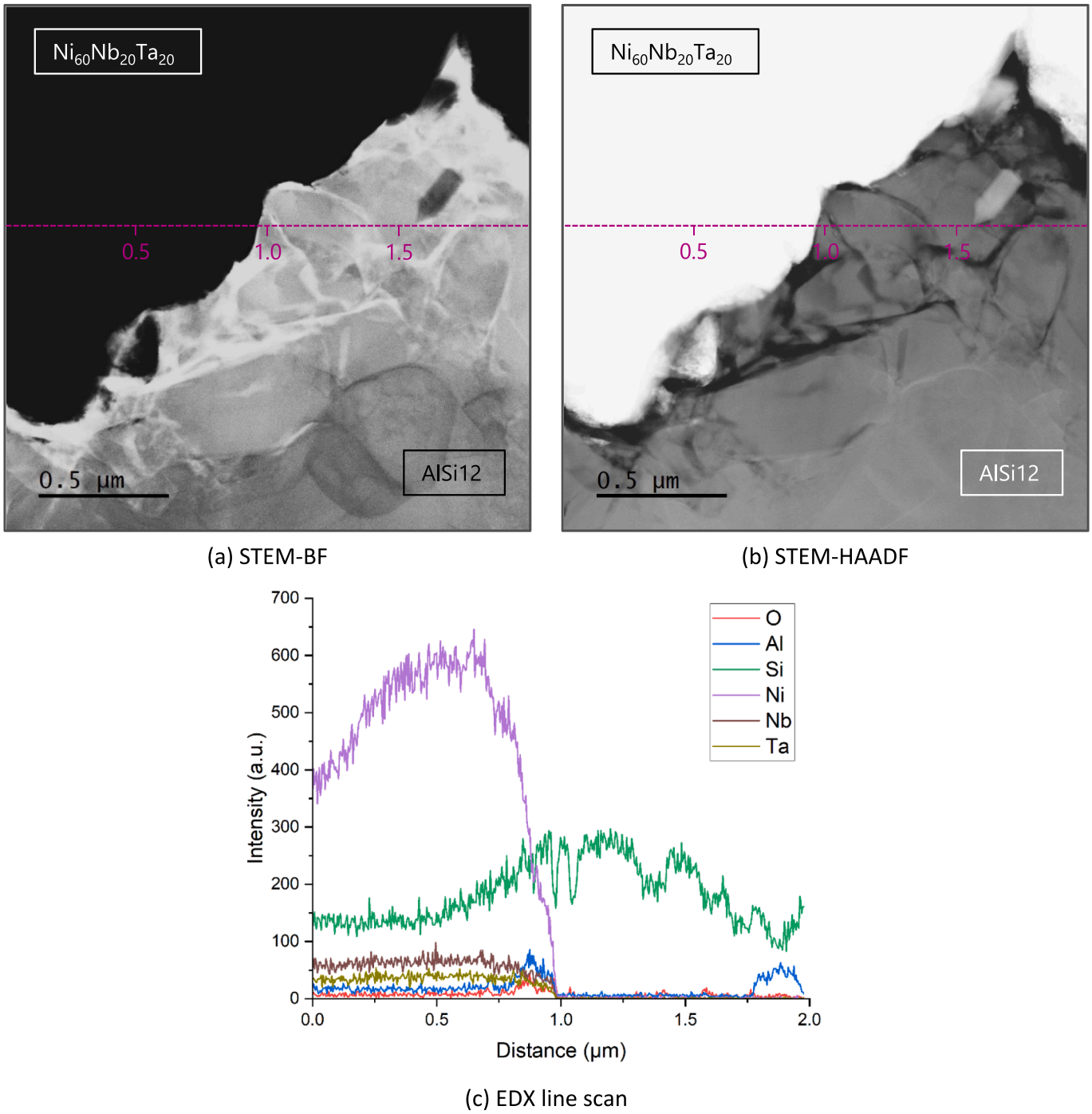

Fig. 7. STEM images of the interface between the metallic glass $Ni_{60}Nb_{20}Ta_{20}$ and the AlSi12-matrix, taken in (a) bright field (BF) and (b) high-angle annular dark field (HAADF) modes with marked EDX scanning line. And (c) the results of the EDX line scan.

transversely to the manufacturing direction ($Ni_{60}Nb_{20}Ta_{20}$-AlSi12-90°). In this work, again a failure due to shear stress in the AlSi12-matrix can be observed, whereas in [15] plastic deformation in the matrix occurs disturbed over the whole sample without a preferred direction. However, in both cases at the end a buckling of the sample instead of shearing can be observed. The slight differences between the failure behavior of the samples in this work compared to [15] are due to the lattice-like compared to the particle-based reinforcement of the metallic glass. However, also in [15] comparatively less debonding occurs at the interfaces between the AlSi12-matrix and the $Ni_{60}Nb_{20}Ta_{20}$ metallic glass.

In general, the main form of deformation in metallic glasses are shear bands which propagate at an angle of 45° to load direction [26]. However, the SEM images of both deformed samples show that most cracks in the $Ni_{60}Nb_{20}Ta_{20}$ phase are parallel to the direction of compression, regardless of whether the loading direction is along or transversely to the manufacturing direction. This is because in composites the failure of individual phases is strongly influenced by interfacial bonding and residual stresses induced during the manufacturing process of the composite [10], the same observation could be made in [15]. Additionally, brittle fracture in the metallic glass phase parallel to load direction can be explained using the model according to [27], which was developed to explain failure in fibers as a function of their orientation. According to this model, compression under compressive load leads to transverse strain in the sample and “in-situ” axial strain

develops in fibers oriented vertically to the load direction. Regarding the failure behavior of the glassy lattice preform in this work, tensile stresses are induced in the lattice struts vertical to load direction leading to fractures parallel to load direction. For fibers oriented parallel to the load direction, failure occurs mainly by fiber buckling [27]. Since buckling is hardly possible in a 3-dimensional structure, damage in the lattice struts parallel to load direction is also initiated by tensile stresses.

Plastic deformation in the matrix phase occurs through brittle fractures in the Si-lamellae and in primary silicon precipitates, growing with increasing load. Similar effects are also observed in unreinforced AlSi alloys under compression load [28]. In [24] a AlSi10Mg alloy was used as matrix material reinforced with an interpenetrating Al_2O_3 foam and investigated by in-situ compression tests. Also, brittle fractures in the precipitates as well as local debonding at the interfaces between the precipitates and the α-aluminum was observed under increasing compression load.

In both samples tested in 0°-direction and 90°-direction the matrix fails due to shear stress in 45° to load direction. Crack propagation in the matrix is restricted in composites by the reinforcement phase [8]. However, in the sample $Ni_{60}Nb_{20}Ta_{20}$-AlSi12-0° shearing of the entire sample can be observed. The development of the shear band probably leads to the significant decrease of the stress after reaching the maximum compressive strength. Even at the end of experiment, the sample is not totally separated through the shear band but still holding together by the matrix phase. This was also observed in [24,29], where fractured ceramic phases were still held together by an interconnected metallic matrix phase. Reason is that the energy is absorbed by plastic deformation and by the hardening of the matrix alloy. Failure at a shear angle of 45° to load direction was also observed in publications with composites with high ceramic reinforcement content [24,30–32].

In the sample $Ni_{60}Nb_{20}Ta_{20}$-AlSi12-90°, the failure behavior is not dominated by shear stress but by normal stress. This is indicated by the composite failing by buckling and not by shear. This means that in this direction the geometry of the metallic glass lattice structure is absorbing the shear stress of the AlSi12-matrix, resulting in a constant stress plateau at maximum compressive strength. This behavior was also observed in interpenetrating MMCs reinforced with a homogenous metallic glass structure in [33,34].

4.2. Interface between $Ni_{60}Nb_{20}Ta_{20}$ metallic glass and AlSi12 matrix

The results of the EDX line scan exhibit a certain intensity of silicon detected in the metallic glass phase. In [35] a diffusion coefficient of only 0.23 x 10^{-22} m^2/s for silicon in metallic glass of composition $Fe_{40}Ni_{40}B_{20}$ was measured at a temperature of 600 K. Additionally, diffusion rates in metallic glasses are in generally very low [36]. Regarding this, the silicon found in the metallic glass is probably not due to diffusion but to misidentification of the peaks. Since the peaks of Si-K line and Ta-M line both appear at 1.7 keV, a peak overlap occurs during the EDX scan resulting in inaccurate identification and quantification by the software [37].

The EDX line scan shows that a primary silicon precipitate has accumulated at the interface. This has already been observed in micrographs of previous investigations on the $Ni_{60}Nb_{20}Ta_{20}$-AlSi12 MMC [22]. This is because the metallic glass acts as a nucleating agent for the silicon, which is often observed in composites with AlSi-based matrix alloys [8,24]. Also, in AlSi10Mg-alloy studies of [38,39] deposition of the silicon at phase boundaries was observed.

At the interface between the $Ni_{60}Nb_{20}Ta_{20}$ metallic glass and AlSi12-matrix a slight increase of oxygen can be observed on the side of the metallic glass phase. This indicates that residual oxygen reacted with the oxygen affine elements Ni and Nb during the manufacturing process of the composite. Studies in [40,41] confirm that a reaction between oxygen and glassy Ni-Nb alloys can occur near the surface at low temperatures. In addition, some aluminum is detected in the EDX line scan overlaying the elements of metallic glass Ni, Nb, and Ta, in an area of 0.25 µm. Therefore, it can be assumed that an interdiffusion layer has formed between the reinforcement and matrix phases during the manufacturing process. However, the reaction layer is comparatively thin, indicating that the metallic glass is resistant to reaction with aluminum, which was also observed in [42,43]. Thin interdiffusion layers normally provide good interfacial bonding and efficient load transfer between the reinforcement and matrix phases in a composite [8,44,45]. During thinning of the TEM lamellae for TEM sample preparation for the EDX measurements, it was observed that the interface between the metallic glass and the AlSi alloy seems to be very brittle and started to crack with decreasing thickness of the lamella. The interface shown in Fig. 7 was one of the few areas still being intact, indicating that the interface is mechanically weak despite the interdiffusion layer.

4.3. Correlation between the interfaces and mechanical failure behavior

In [8], it is described that two types of bonding at interfaces in MMCs exist: mechanical and chemical bonding. Mechanical bonding occurs when the reinforcing phase has a rough surface, enabling mechanical keying with the matrix. A chemical bond is formed when a solid solution and/or chemical compound is formed at the interface by diffusion and reaction of the elements. Normally, MMCs with an amorphous reinforcement phase and metallic matrix exhibit good interfacial bonding due to the metallic character of both phases [8,16–18]. In this work, an interdiffusion layer and thus a chemical bond could have been formed at the interfaces between the reinforcing $Ni_{60}Nb_{20}Ta_{20}$ metallic glass and AlSi12-matrix, but it is very weak and brittle and therefore does not provide a consistently good interfacial bonding. However, also a rough surface at the interface is observed in the STEM images in Fig. 7, indicating mechanical bonding between the two phases. This is confirmed by the in-situ results where little interfacial debonding is observed. The fractures do not propagate exactly at the interface but in the matrix close to the interface and it can be observed that matrix material sticks to the surface of the metallic glass. Another weakness of the interface is the deposition of the primary silicon precipitates to the metallic glass phase, in these areas it can be observed that cracks propagate directly along the interfaces. Fig. 8 shows a hardness indentation that was performed on the interface between the $Ni_{60}Nb_{20}Ta_{20}$ metallic glass and AlSi12-matrix for further investigations of the interfacial bonding. Crack growth can be observed at the corners of the indent between the metallic glass and the AlSi12-matrix. On closer inspection, it is evident that the cracks grow only along the interface of the Si-lamellae and primary silicon precipitates to the metallic glass phase and α-aluminum and do not further propagate. This was also observed in [15] and indicates good interfacial

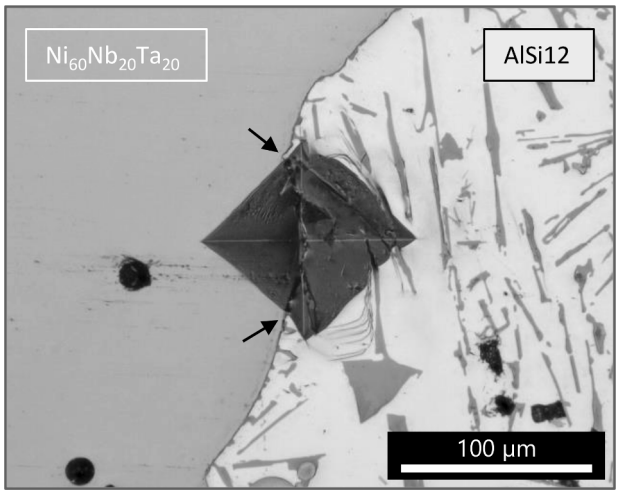

Fig. 8. Hardness indentation on the interface between the $Ni_{60}Nb_{20}Ta_{20}$ metallic glass and AlSi12-matrix.

adhesion, confirming the assumptions made.

5. Conclusions

In this work an interpenetrating MMC with a $Ni_{60}Nb_{20}Ta_{20}$ metallic glass reinforcement phase and a AlSi12-matrix was investigated in and transversely to manufacturing direction by in-situ compression tests in a SEM and EDX measurements in a TEM. To the author's best knowledge, this is the first time the in situ mechanical failure behavior of this material system and its correlation with interfacial adhesion have been investigated. The following conclusions can be drawn.

The sample tested in manufacturing direction ($Ni_{60}Nb_{20}Ta_{20}$-AlSi12-0°) exhibits a different failure behavior and higher compressive strength than the sample tested transversely to manufacturing direction ($Ni_{60}Nb_{20}Ta_{20}$-AlSi12-0°) indicating an anisotropic failure behavior.

Both samples show shear stress failure in the matrix phase and normal stress failure in the metallic glass phase. But whereas the failure behavior in the 0°-sample is dominated by shear stress resulting in shearing of the whole sample, the 90°-sample is dominated by normal stress resulting in buckling of the sample in the end of experiment.

The metallic glass phase fails due to brittle fractures along the load direction in both samples and the matrix due to plastic deformation. The plastic deformation occurs through brittle fractures in the Si-lamellae and the primary silicon precipitates as well as debonding on the interfaces between the silicon and α-aluminum.

Debonding at the interface between the metallic glass and matrix occurs less in 0°-direction than in 90°-direction with the mechanical interface strength being relatively low.

The STEM images showing a rough interface between the metallic glass and matrix phase. The EDX line scan across the interface shows that some reaction between oxygen and the elements Ni and Nb of the metallic glass took place. Additionally, a thin interdiffusion layer could have been formed through a reaction between the α-aluminum and the elements of the metallic glass.

The sample preparation for the TEM investigations shows that the interfaces between the metallic glass and matrix are brittle. Consequently, the good interfacial bonding, that is observed, is both based on mechanical interlocking due to the roughness of the interface as well as due to the shrinkage of the aluminum melt after infiltration.

To sum up, the manufacturing method presented delivers mechanically performing interpenetrating composites featuring an anisotropy that might be controlled by the preform structure with a sufficient interface bonding.

CRediT authorship contribution statement

Kerstin Dittmann: Conceptualization, Investigation, Writing – original draft. **Robert Gruhl:** Investigation, Writing – original draft. **Anna Trauth:** Supervision, Writing – review & editing. **Kay André Weidenmann:** Funding acquisition, Supervision, Writing – review & editing.

Declaration of competing interest

The authors declare that they have no known competing financial interests or personal relationships that could have appeared to influence the work reported in this paper.

Data availability

Data will be made available on request.

Acknowledgments

The authors are thankful to Fraunhofer Institute IFAM (Dresden, Germany) and Nanoval GmbH & Co.KG (Berlin, Germany) for producing the metallic glass alloy and powder. Further, the authors are especially thankful to Steffen Czink from the research group "Production and Component Behavior" (Institute of Applied Materials - Materials Science and Engineering) at Karlsruhe Institute of Technology for carrying out the LPBF process. Also, special thanks to the Center for Electronic Correlations and Magnetism (Experimental Physics VI) at Augsburg University for providing their TEM and FIB equipment. The financial support of the German Research Foundation (DFG) within the project WE 4273/19-1 is gratefully acknowledged.

References

[1] Suryanarayana C. Metallic glasses. Bull Mater Sci 1984;6(3):579–94. https://doi.org/10.1007/BF02744086.
[2] Inoue A, Shen B, Koshiba H, et al. Cobalt-based bulk glassy alloy with ultrahigh strength and soft magnetic properties. Nat Mater 2003;2(10):661–3. https://doi.org/10.1038/nmat982.
[3] Schroers J. Processing of bulk metallic glass. Adv Mater 2010;22(14):1566–97. https://doi.org/10.1002/adma.200902776.
[4] Ashby M, Greer A. Metallic glasses as structural materials. Scr Mater 2006;54(3):321–6. https://doi.org/10.1016/j.scriptamat.2005.09.051.
[5] Scudino S, Surreddi KB, Sager S, Sakaliyska M, Kim JS, Löser W, et al. Production and mechanical properties of metallic glass-reinforced al-based metal matrix composites. J Mater Sci Lett 2008;43(13):4518–26. https://doi.org/10.1007/s10853-008-2647-5.
[6] Dudina DV, Georgarakis K, Li Y, Aljerf M, LeMoulec A, Yavari AR, et al. A magnesium alloy matrix composite reinforced with metallic glass. Compos Sci Technol 2009;69(15–16):2734–6. https://doi.org/10.1016/j.compscitech.2009.08.001.
[7] Siegrist ME, Löffler JF. Bulk metallic glass–graphite composites. Scr Mater 2007;56(12):1079–82. https://doi.org/10.1016/j.scriptamat.2007.02.022.
[8] Chawla N, Chawla KK. Metal matrix composites. Boston, MA: Springer, US; 2006.
[9] Clarke DR. Interpenetrating phase composites. J Am Ceram Soc 1992;75(4):739–58. https://doi.org/10.1111/j.1151-2916.1992.tb04138.x.
[10] Jayalakshmi S, Gupta M. Metallic amorphous alloy reinforcements in light metal matrices. Cham: Springer; 2015.
[11] Polmear IJ, StJohn D, Nie J-F, Qian M. Light alloys: metallurgy of the light metals. 5th ed. Kidlington, Oxford, Cambridge, MA: Butterworth-Heinemann; 2017.
[12] Dudina DV, Georgarakis K, Aljerf M, Li Y, Braccini M, Yavari AR, et al. Cu-based metallic glass particle additions to significantly improve overall compressive properties of an al alloy. Compos A Appl Sci Manuf 2010;41(10):1551–7. https://doi.org/10.1016/j.compositesa.2010.07.004.
[13] Lichtenberg K, Weidenmann KA. Innovative aluminum based metallic glass particle reinforced MMCs produced by gas pressure infiltration. Mater Sci Forum 2015;825–826:101–8. https://doi.org/10.4028/www.scientific.net/MSF.825-826.101.
[14] Scudino S, Liu G, Prashanth KG, Bartusch B, Surreddi KB, Murty BS, et al. Mechanical properties of al-based metal matrix composites reinforced with zr-based glassy particles produced by powder metallurgy. Acta Mater 2009;57(6):2029–39. https://doi.org/10.1016/j.actamat.2009.01.010.
[15] Lichtenberg K. Metal matrix composite reinforced with metallic glass (Ni60Nb20Ta20): fabrication and Characterization [PhD Thesis]. Karlsruhe, Germany: Karlsruhe Institute of Technology; 2017.
[16] Blank-Bewersdorff M, Köster U, Steinbrink G. Interfaces with improved adhesion in metal matrix/metallic glass composites. J Mater Sci Lett 1989;8(7):796–8. https://doi.org/10.1007/BF01730141.
[17] Yu P, Kim KB, Das J, Baier F, Xu W, Eckert J. Fabrication and mechanical properties of Ni–Nb metallic glass particle-reinforced al-based metal matrix composite. Scr Mater 2006;54(8):1445–50. https://doi.org/10.1016/j.scriptamat.2006.01.001.
[18] Jayalakshmi S, Gupta S, Sankaranarayanan S, Sahu S, Gupta M. Structural and mechanical properties of Ni60Nb40 amorphous alloy particle reinforced al-based composites produced by microwave-assisted rapid sintering. Mater Sci Eng A 2013;581:119–27. https://doi.org/10.1016/j.msea.2013.05.072.
[19] Takayama S, Fehrman RG. Composite metallic glass wires. J Mater Sci 1980;15(2):532–4. https://doi.org/10.1007/BF02396811.
[20] Blank-Bewersdorff M, Köster U, Bewernick G. Metallic amorphous/crystalline interfaces. In: Ishida H, editor. Controlled Interphases in Composite Materials: Proceedings of the Third International Conference on Composite Interfaces (ICCI-III) held on May 21-24, 1990 in Cleveland. Ohio, USA: Dordrecht: Springer Netherlands; 1990.
[21] Dittmann K, Czink S, Dietrich S, Trauth A, Weidenmann KA. Laser-Based Additive Manufacturing and Characterization of an Open-Porous Ni-Based Metallic Glass Lattice Structure (Ni60Nb20Ta20). 3D Printing and Additive Manufacturing 2022. 10.1089/3dp.2022.0118.
[22] Dittmann K, Trauth A, Weidenmann KA. Manufacturing and characterization of an interpenetrating metal matrix composite reinforced with a 3D-printed metallic glass lattice structure (Ni60Nb20Ta20). Compos Struct 2024;327:117697. https://doi.org/10.1016/j.compstruct.2023.117697.
[23] Mondolfo LF. Aluminum alloys: structure and properties. London and Boston: Butterworths; 1976.

[24] Morbitzer PC, Schukraft J, Lohr C, Weidenmann KA. In-situ SEM investigation on the damage behavior of an interpenetrating metal ceramic composite. Compos Struct 2023;321:117278. https://doi.org/10.1016/j.compstruct.2023.117278.
[25] Wang Z, Scudino S, Stoica M, Zhang W, Eckert J. Al-based matrix composites reinforced with short fe-based metallic glassy fiber. J Alloy Compd 2015;651:170–5. https://doi.org/10.1016/j.jallcom.2015.08.098.
[26] Johnson WL. Bulk glass-forming metallic alloys: science and technology. MRS Bull 1999;24(10):42–56. https://doi.org/10.1557/S0883769400053252.
[27] Wanner A, Arzt E. Short fiber reinforced metal matrix composites – investigations by acoustic emission and neutron diffraction. In: Busse G, editor. Damage and its evolution in fiber-composite materials: Simulation and non-destructive evaluation. Stuttgart: ISD-Verl; 2006. p. 193–202.
[28] Mocellin A, Fougeres R, Gobin PF. A study of damage under tensile loading in a new al-si-fe alloy processed by the osprey route. J Mater Sci 1993;28(18):4855–61. https://doi.org/10.1007/BF00361147.
[29] Bandyopadhyay A, Atisivan R, Kuhn G, Yeruva S. Mechanical properties of interconnected phase alumina-al composites 24. The University of Texas at Austin; 2000.
[30] Scherm F, Völkl R, Neubrand A, Bosbach F, Glatzel U. Mechanical characterisation of interpenetrating network metal–ceramic composites. Mater Sci Eng A 2010;527(4–5):1260–5. https://doi.org/10.1016/j.msea.2009.09.063.
[31] San Marchi C, Kouzeli M, Rao R, Lewis JA, Dunand DC. Alumina–aluminum interpenetrating-phase composites with three-dimensional periodic architecture. Scr Mater 2003;49(9):861–6. https://doi.org/10.1016/S1359-6462(03)00441-X.
[32] Wang F, Zhang X, Wang Y, Fan Q, Li G. Damage evolution and distribution of interpenetrating phase composites under dynamic loading. Ceram Int 2014;40(8):13241–8. https://doi.org/10.1016/j.ceramint.2014.05.031.
[33] Sun Y, Zhang HF, Wang AM, et al. Mg-based metallic glass/titanium interpenetrating phase composite with high mechanical performance. Appl Phys Lett 2009;95(17):171910. https://doi.org/10.1063/1.3257699.
[34] Zhang H, Wang A, Li H, et al. Quasi-static compressive property of metallic glass/porous tungsten bi-continuous phase composite. J Mater Res 2006;21(6):1351–4. https://doi.org/10.1557/jmr.2006.0166.
[35] Sharma SK, Macht M-P, Naundorf V. Impurity diffusion in the metallic glass Fe40Ni40B20 measured by SIMS. In: Mazzoldi P, editor. Modifications induced by irradiation in Glasses: Proceedings of Symposium F on Chemical and Physical Modifications Induced by Irradiation in Glases of the 1991 E-MRS fall conference, Strasbourg, France, November 5 - 7, 1991. Amsterdam: North-Holland; 1992, p. 85–90.
[36] Akhtar D, Cantor B, Cahn RW. Diffusion in metallic glasses. Bull Mater Sci 1985;7(1):3–13. https://doi.org/10.1007/BF02744252.
[37] Suzuki M, Rohde D. Resolving Overlapping Peak Problems with NORAN System 7 Spectral Imaging Software, Application Note: 51188, Thermo Fisher Scientific, Madison, WI, USA (2008); Available from: https://assets.thermofisher.com/TFS-Assets/CAD/Application-Notes/D10051~.pdf.
[38] Aboulkhair NT, Tuck C, Ashcroft I, Maskery I, Everitt NM. On the precipitation Hardening of selective laser melted AlSi10Mg. Metall Mater Trans A 2015;46(8):3337–41. https://doi.org/10.1007/s11661-015-2980-7.
[39] Zhou Le, Mehta A, Schulz E, McWilliams B, Cho K, Sohn Y. Microstructure, precipitates and hardness of selectively laser melted AlSi10Mg alloy before and after heat treatment. Mater Charact 2018;143:5–17. https://doi.org/10.1016/j.matchar.2018.04.022.
[40] Song Z, Tan D, He F, Bao X. Surface segregation behaviors of amorphous Ni65Nb35 alloy under oxidation in O2 at various temperatures. Appl Surf Sci 1999;137(1–4):142–9. https://doi.org/10.1016/S0169-4332(98)00466-8.
[41] Gallino I, Busch R, Yim HC, Jastrow L, Köster U. High temperature oxidation of the refractory alloy glass Nb35Ni60Sn5. J Alloy Compd 2007;434–435:225–8. https://doi.org/10.1016/j.jallcom.2006.08.101.
[42] Yu P, Zhang LC, Zhang WY, Das J, Kim KB, Eckert J. Interfacial reaction during the fabrication of Ni60Nb40 metallic glass particles-reinforced al based MMCs. Mater Sci Eng A 2007;444(1–2):206–13. https://doi.org/10.1016/j.msea.2006.08.077.
[43] Lee M. Fabrication of Ni–Nb–Ta metallic glass reinforced al-based alloy matrix composites by infiltration casting process. Scr Mater 2004;50(11):1367–71. https://doi.org/10.1016/j.scriptamat.2004.02.038.
[44] Needleman A, Nutt SR, Suresh S, Tvergaard V. Matrix, reinforcement, and Interfacial failure. In: Suresh S, Mortensen A, Needleman A, editors. Fundamentals of metal-matrix composites. Boston: Butterworth-Heinemann; 1993. p. 233–50.
[45] Wang Z, Georgarakis K, Nakayama KS, Li Y, Tsarkov AA, Xie G, et al. Microstructure and mechanical behavior of metallic glass fiber-reinforced al alloy matrix composites. Sci Rep 2016;6:24384. https://doi.org/10.1038/srep24384.